Title: Environmental Hg vapours adsorption and detection by using functionalized gold nanoparticles network

Authors: Andrea Bearzotti, Paolo Papa, Antonella Macagnano, Emiliano Zampetti, Iole Venditti, Raoul Fioravanti, Laura Fontana, Roberto Matassa, Giuseppe Familiari, Ilaria Fratoddi

PII: S2213-3437(18)30392-0
DOI: https://doi.org/10.1016/j.jece.2018.07.013
Reference: JECE 2508

To appear in:

Received date: 2-3-2018
Revised date: 31-5-2018
Accepted date: 7-7-2018

Please cite this article as: Bearzotti A, Papa P, Macagnano A, Zampetti E, Venditti I, Fioravanti R, Fontana L, Matassa R, Familiari G, Fratoddi I, Environmental Hg vapours adsorption and detection by using functionalized gold nanoparticles network, *Journal of Environmental Chemical Engineering* (2018), https://doi.org/10.1016/j.jece.2018.07.013

Environmental Hg vapours adsorption and detection by using functionalized gold nanoparticles network.

Andrea Bearzotti[a*], *Paolo Papa*[a,b], *Antonella Macagnano*[a], *Emiliano Zampetti*[a], *Iole Venditti*[d], *Raoul Fioravanti*[b], *Laura Fontana*,[b] *Roberto Matassa*[c], *Giuseppe Familiari*[c], *and Ilaria Fratoddi*[b*]

[a] CNR, Institute of Atmospheric Pollution Research, Via Salaria, 300, Monterotondo, 00015 Rome, Italy.

[b] Department of Chemistry, Sapienza University of Rome, Piazzale Aldo Moro 5, 00185, Rome, Italy.

[c] Department of Anatomical, Histological, Forensic and Orthopaedic Sciences, Section of Human Anatomy , Sapienza University of Rome, Via A. Borelli 50, 00161 Rome, Italy.

[d] Department of Sciences, Roma Tre University of Rome, Via della Vasca Navale, 79, 00100, Rome, Italy.

Corresponding authors. *E-mail addresses:* a.bearzotti@iia.cnr.it (A. Bearzotti),

Ilaria.Fratoddi@uniroma1.it (I. Fratoddi)

Graphical abstract

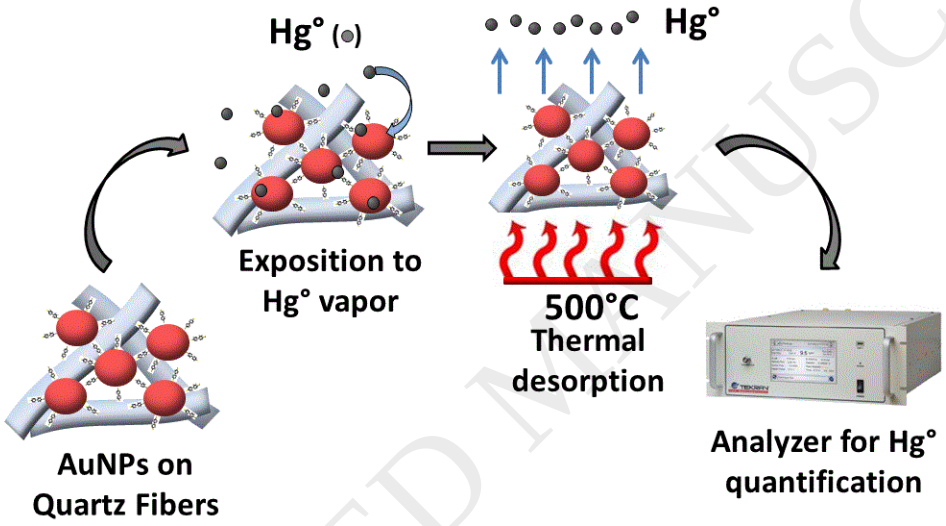

Highlights

- Environmental gaseous elemental mercury detection
- Dithiol ligands functionalized gold nanoparticles
- High and stable mercury uptake

- Monitoring of environmental and indoor vapour mercury
- Ready for large-scale measurement campaigns

ABSTRACT.

Adsorption and detection of environmental total gaseous mercury (TGM) was studied by using gold nanoparticles (AuNPs) on purpose functionalized with dithiol ligands, *i.e.* Biphenyl-4,4′-dithiol (BI) or *p*-Terphenyl-4,4″-dithiol (TR), suitable for nanoparticles based network formation. AuNPs-BI and AuNPs-TR with size 6-8 nm were deposited onto quartz fibres and used as adsorbent materials for the detection of TGM, both indoor for adsorption studies, at defined concentrations (~4.5 ng m^{-3} Hg), and outdoor, at the vapour mercury concentration of the environmental countryside (~1.5 ng m^{-3} Hg). The role of relative humidity (RH) in the absorption process has been observed. A high Hg adsorption capability, also when exposed to sub ppb concentration, has been observed. A cold vapour atomic fluorescence spectroscopy (CVAFS) detector was used to determine gaseous mercury concentrations lower than 2 ng m^{-3}, with a robust and reproducible procedure. Moreover, the use of quartz fibres substrate covered with AuNPs-BI or AuNPs-TR, and used for more than thirty times during the experiments, makes them competitive in the use in large-scale measurement campaigns.

KEYWORDS: mercury vapour monitoring, gold nanoparticles, outdoor monitoring, sensing device

1. Introduction

Elemental Mercury (Hg°) is one of the trace elements emitted into the atmosphere [1], well known for its toxicity and hazardous effects, even at low levels [2]. Emission sources for mercury include both natural processes and anthropogenic sources. Moreover, its concentration in air strongly depends from the volatility degrees of its compounds, which are related to the surrounding temperature. Current emissions of mercury from natural and anthropogenic sources include gold mining and processing, fuel combustion, catalysis in plastics or batteries production [3]. Mercury can be present in the atmosphere in three different forms: the gaseous elemental mercury Hg° (GEM), which can be converted into gaseous oxidized mercury Hg(II) (GOM) and particle bound mercury HgP(2.5) (PBM) [4]. These three forms can be considered as the total gaseous mercury (TGM), although the predominant form in the atmosphere is composed by GEM, which represents approximately the 98-99% of the TGM [5]. Generally, in the atmosphere the average concentration of the TGM ranges from 1.5–1.7 ng m^{-3} to 1.1–1.3 ng m^{-3}, respectively referred to the northern and southern hemisphere [6,7], with some variation in the polar regions [8]. Gaseous mercury concentration is under increasing monitoring and study, trying to understand its behaviour, its environmental cycle and the bio-accumulation in the food chain [9,10]. Currently, the detection and quantification of the environmental gaseous mercury is carried out by analyser systems [11,12], mostly based on the usage of reliable instruments, as Tekran® 1130/1135/2537. However, these analysis tools, while providing a fine temporal resolution through cyclic sampling, have a limited spatial resolution and high management costs. This limits their use also due to the need for management by expert personnel, hyper-pure argon cylinders and electric power supply. All this makes them unsuitable for use in remote and/or poorly civilized areas.

To overcome these limitations, researchers have developed alternative measurement systems, in particular based on the use of passive air concentrators [13,14]. The main advantage of these concentrators in the detection of gaseous mercury is the possibility of using them in a large distribution area, providing a high spatial sampling resolution. A common drawback is, in general, that these components can only be used once [15,16], with relatively high sampling costs.

The adsorbent ability of passives is based on the capacity of some noble metals to have an adsorption of vapour mercury leading to the formation of an amalgam. In particular, gold is a well-known mercury adsorbent thanks to its strong chemical affinity and gold films were recently used for Hg detection, both as passive and transducer layer. For example, Au films were used in quartz crystal microbalance (QCM) devices [17] or in optical based measurements [18] generally with fast response time and low detection limits. Surface acoustic wave (SAW) sensors with a gold film sensitive layer were also used in the presence of different vapour organic chemicals (VOCs), demonstrating a detection limit towards Hg vapour of 4 ppbv at 75°C, with limited cross-sensitivity effect when the relative humidity content was increased [19]. Carbon supported Au nanoparticles were used as sorbent composites for Hg capture, giving interesting performances even in the presence of O_2, NO, SO_2 and HCl [20] and the use of nano-engineered surfaces both as sensor and for Hg removal is a topic of great industrial interest [21].

The interaction of gold films with mercury has been extensively studied in literature [22,23]. It has been hypothesized that, starting from an initial adsorption of mercury on the gold surface, islands are formed with the successive appearance of dendritic structures during the amalgamation process [24,25]. It has also been observed that a high amount of grain boundaries,

typical of nanostructured materials, results in a greater efficiency of the reactivity of the gold surface, resulting in a generally faster and more efficient adsorption and mercury detection [26].

In general, nanomaterials and nanocomposites allow to building up particular 3D nanoarchitectures with large surface-to-volume ratio, which lead to high catalytic activity with the surrounding environment [27,28,29]. In particular, AuNPs whose average size falls in the range from some hundreds nanometers, can be considered one of the leading materials in emerging fields such as catalysis or biocatalysis [30,31], optoelectronics [32,33], nanomedicine [34,35,36] or drug delivery [37], thanks to their size-dependent properties and their chemical stability [38,39]. In particular, in recent years the use of AuNPs as chemical sensors garnered considerable attention for the potential to obtain fast and selective devices. For example, gold covered polystyrene nano spheres were used as QCM sensors for the detection of Hg° with high sensitivity and selectivity, also due to their long-range interspatial order and high number of surface defect formation [40]. Quite recently, gold nano rods were used for mercury vapour plasmonic sensors, by studying the surface plasmon resonance (SPR) shift of gold nano rods upon exposure towards mercury vapour [41] and silver nanoparticles (AgNPs) embedded into a polymer film were able to detect either Hg°, Hg(I) and Hg(II) species [42]. AuNPs were used for reusable Hg° sensor, showing a reduction of about 50% in sensitivity upon thermal treatment cycles [43].

In the present work, we utilized gold nanoparticles (AuNPs) functionalized with the bifunctional thiols Biphenyl-4,4′-dithiol (BI) or p-Terphenyl-4,4″-dithiol (TR), able to self-assemble in a stable network of interconnected nanoparticles as adsorbent material for the detection of TGM, both indoor (expositing the material to defined concentrations) and outdoor (at the vapour mercury concentration of the environmental countryside) for adsorption studies. AuNPs-BI and

AuNPs-TR were deposited onto quartz fibres, and used in more than 30 thermal desorption cycles at 500°C [44], showing over time a stable response and a high sensitivity at sub ppb concentration (lower than 2 ng m^{-3}), also in the presence of interfering agents such as relative humidity.

2. Experimental

2.1 Materials

Solvents and reagents were purchased from Sigma-Aldrich: Tetrachloroauric (III) acid trihydrate ($HAuCl_4 \cdot 3H2O$), Tetraoctylammonium bromide (TOAB), Sodium borohydride ($NaBH_4$), Biphenyl-4,4′-dithiol (BI) and p-Terphenyl-4,4″-dithiol (TR), Dichloromethane, Chloroform, Ethanol, Toluene, Petroleum Ether.

2.2 Instruments

UV-Vis absorption spectra were run in dichloromethane by using quartz cells, with a Varian Cary 100 Scan UV-Vis spectrophotometer. FTIR spectra were recorded with a Bruker Vertex 70 instrument using KRS-5 cells, in the 4000–400 cm-1 range and the samples have been prepared as cast films or from Nujol mulls. Variable Pressure Scanning Electron Microscopy (VP-SEM, Hitachi SU-3500) at high vacuum mode supported by dual energy dispersive X-ray spectroscopy (dEDX) detectors in parallel configuration (Bruker, XFlash® 6|60) able to high sensitivity elemental analysis has been employed to analyse AuNPs deposited on surface of quartz fibres films. A Scilogex refrigerated microcentrifuge was used for purification of AuNPs samples (5000 rpm, 20 min, 4°C, 5× with ethanol). Deionized water was obtained from Zeener Power I Scholar-UV (18.2 MΩ). Tekran® Model 2505 (Tekran Instruments Corporation, Toronto, CA-ON) mercury vapour calibration unit primary source, has been employed to

generate defined selected quantities and concentrations of mercury vapour. Tekran® Model 2537A ambient mercury vapours analyser was used to control external concentrations and to measure mercury adsorbed on samples. Atomic force microscopy (AFM) images were obtained using a Nanosurf Flex AFM.

2.3 AuNPs synthesis and characterizations

The AuNPs synthesis has been carried out starting from tetrachloroauric acid with a well assessed two phase's reduction procedure [45,46], optimized for dithiol ligands [47,48]. Experimental parameters have been optimized to obtain small nanoparticles with low dispersity in dimension using a 3:1 metal:sulfur molar ratio for the synthesis of both AuNPs-BI and AuNPs-TR samples.

As a typical procedure, the AuNPs-TR synthesis is herein reported: an aqueous solution of $HAuCl_4 \cdot 3H_2O$ (0.0801 g, 2.00 x 10^{-4} mol) in freshly prepared deionized water (5 mL), was mixed with a solution of tetraoctylammonium bromide (TOAB) (0.1200 g, 2.00 x 10^{-4} mol) in toluene (5 mL). The two-phase mixture was vigorously stirred until all the Au^{3+} were transferred into the organic layer and a solution of TR (0.0100 g, 0.33 x 10^{-4} mol) in toluene (3 mL) was then added. A NaBH4 deionized water solution (0.0796 g, 2.00 x 10^{-3} mol) in 2 mL deionized water) was added under vigorous stirring. After 3 h the organic phase was separated, and washed with water. The organic phase was reduced to 2 mL in a rotary evaporator, and 40 mL of ethanol were added. The mixture was kept overnight at -18°C and then centrifuged at 5000 rpm for 15 min at 4°C, in order to remove the excess of thiol and TOAB. The supernatant was eliminated and the precipitate was washed by centrifugation at 13400 rpm for 10 min with ethanol at 4°C for 10 times. After the removal of the supernatant, a red-violet suspension of AuNPs-TR was

obtained (yield 30% wt). AuNPs-TR main characterization: λ_{max} (nm, CH_2Cl_2) 585; FTIR (film, cm^{-1}): 2920, 2853, 1588, 1456, 1371, 1078, 993, 800, 699. Two comparison spectra of both AuNPs-BI and AuNPs-TR are reported in the Supporting Information figure S1 and S2 together with the picture of the two materials dispersed in dichloromethane, figure S3.

2.4 Adsorbent material preparation

A thin disc of quartz wool (Whatman© quartz filters) consisting of quartz fibres (QF) was used as substrate support. AuNPs-BI and AuNPs-TR were deposited on substrates by casting 100 µL of a dichloromethane solution (at concentration 1 mg/mL). A series of ten samples for each kind of nanostructured materials were obtained with the purpose to investigate the adsorbing properties. The interaction area containing the AuNPs was a circle spot of 13 mm in diameter, slightly smaller than the substrate with a diameter of 17 mm and thickness of 0.5 mm. With this preparation an active total surface of approx. 130 mm^2 was obtained, as reported in the Supporting Information figure S4.

After the deposition process, the samples were dried for two hours in an oven at 40°C and then were thermally treated at 500°C for 5 mins in order to avoid possible environmental mercury contamination with the solvent or volatile organic elements adsorbed during sample preparation process. The sensing devices were housed in a sealed glass holder, previously blown with dry nitrogen.

2.5 Exposition towards vapour mercury

AuNPs-BI-QF and AuNPs-TR-QF devices were tested in order to evaluate their performance both in indoor controlled concentration exposition measurements and in outdoor exposition (at environmental countryside mercury concentration). To analyse these samplers, a suitable thermal desorption system connected to a mercury analyser was developed.

The system is made of different parts here below reported:

1) gas delivering system: a quartz crucible necessary to hold the sample which has to be inserted in an oven for the heat treatment.

2) furnace: able to reach temperatures of 500°C (the desorption temperature set to release the mercury adsorbed on the AuNPs).

3) Tekran® 2537A: instrument equipped with a cold vapour atomic fluorescence spectrophotometer (CVAFS) detector, necessary to quantify the TGM released from the sample.

A representative scheme of the system is available in the Supporting Information figure S5.

In order to characterize the absorption behaviour of the materials (both AuNPs-BI and AuNPs-TR samplers), different expositions and measurements were carried out, evaluating the adsorption performances towards the collection of gaseous vapour mercury at defined concentrations and time expositions. For these purposes, we used a test chamber made of quartz (with a volume of 8 cm^3) and a primary mercury source (Tekran® 2505 mercury vapour primary calibration unit) to generate constant amounts of elemental mercury. Moreover, a Hamilton® gastight syringe to inject vapour mercury in the chamber was used.

A first set of measurements concerned the evaluation of the maximum mercury uptake capacity of these samplers in vapour mercury saturation conditions. This study was done using an AuNPs-

TR sampler, exposing it to different lapses of time at a saturated mercury vapour concentration at 20°C, equal to 13.176 mg m^{-3} (1.6 ppm), according to the Dumarey equation [49,50]:

$$\gamma Hg = \frac{D}{T}\, 10^{-\left(A+\left[\frac{B}{T}\right]\right)}$$

where γHg is the saturated mass concentration of mercury in the air expressed in ng/mL, while D, B and A are constants and T is the temperature expressed in K. Afterwards we performed fixed amount of mercury for different exposure times. In this case, an amount of mercury, equal to 1.995 ng Hg° was injected in the exposition chamber containing the sampler to perform expositions with different lengths of time (15, 30, 90 and 120 minutes), desorbing and measuring the sample after each exposition. With this experimental set-up we were able to measure the adsorption rate of the total adsorbed mercury. In order to evaluate the possible changes in the adsorption characteristics of the AuNPs-TR, cyclic measurements of a first exposure and a subsequent desorption were performed considering a series of more than 35 consecutive measurements. The real environmental conditions were simulated using a series of 20 adsorbing samples (10 AuNPs-TR-QF and 10 AuNPs-BI-QF) placed in an aluminium sample-holder grid at a distance of at least 2 cm each other.

The surface of the samples were oriented with the adsorbent surface facing downwards in order to avoid undesirable dust deposition effects and placed in another holder suitable for the exposition, as reported in the Supporting Information, figure S5.

During the outdoor exposition, the mercury concentration level was monitored by the analyser Tekran® 2537A to obtain accurate information about the exposure and possible changing conditions of the experimental environment. Through these measurements, a stable background mercury concentration of 1.5 ng m^{-3} (± 0.4 ng m^{-3}) was measured. During the exposition the

TGM adsorbed on the samplers (both AuNPs-BI and AuNPs-TR) was measured and quantified progressively after 1, 7, 14, 21, 28 and 56 days.

3. Results and Discussion

The modern wet-chemistry approach for the production of gold nanoparticles (AuNPs) received an increasing interest in recent years for the challenging opportunity of isolating stable interconnected networks suitable for solid state applications [51,52]. The structural complexity and crystal growth of these covalent aggregates of nanoparticles was recently studied [53] and their structural thermal stability was investigated [54]. AuNPs have been prepared in the presence of the π-conjugated dithiol BI or TR, whose chemical structures are shown in Figure 1a-c, together with the reaction scheme. The use of the chemical reduction procedure of the $HAuCl_4$ in the presence of bifunctional BI and TR thiols and sodium borohydride as reducing agent was optimized in order to achieve a stable and soluble AuNPs based network. The obtained nanoparticles were soluble in common organic solvents such as dichloromethane and toluene and their stability in solution was monitored up to one month. The formation of the AuNPs was monitored by means of UV-Vis and morphology characterizations. In particular, the molar ratio 3:1 between Au/S was fixed and the UV-Vis characterization evidenced a SPR broad absorption at about 600 nm, both for AuNPs-BI and AuNPs-TR, red shifted with respect to the typical SPR band of isolated AuNPs found at about 520 nm [55,56]. This shift strongly depends on the interaction among NPs and intercoupling effects [57]. It can be used among others, for chemical and biochemical sensing in complex NPs architectures [58] and for electron transport studies [59]. It is noteworthy that thanks to the high chemical-structure stability, the AuNPs can be stored in solution until its applicative use. In order to check the behaviour of the nanoparticles under thermal stress, an AFM study in non-contact mode was carried out on AuNPs-BI and

AuNPs-TR drop-cast deposited onto silicon substrate, before and after the thermal treatment at 500°C.

As it is possible to observe in Figure 2a for AuNPs-TR sample, uniformly distributed AuNPs with maximum diameter of about 6 nm can be noted in the pristine material. After a thermal treatment at 500°C it is possible to observe a slight increase in AuNPs diameter and the formation of some aggregates, due to a possible merging of vicinal AuNPs. The mean diameter of the NPs was maintained below 15 nm. This preliminary study allowed considering the AuNPs as stable in the used thermal stressing conditions.

3.1 Samplers exposure to environmental mercury vapour

The sensing properties of a hybrid device based on AuNPs deposited onto quartz fibres were characterized before and after exposition to elemental gas mercury and after thermal treatment. A study of the uptake capability and the morphological behaviour of the AuNPs samplers was carried out sampling the atmospheric gaseous mercury present in the surrounding countryside of our research centre located in a rural area at North-East of Rome (Italy), away from major anthropogenic sources of air pollutants, with a rather low and stable mean values of TGM over time, in the order of 1.5 ± 0.4 ng m^{-3} of Hg. During the sampling measurements weather parameters (wind speed, temperature, relative humidity and rainfall) were monitored valuating possible influences on the sensing measurements.

The adsorbent samplers utilized for these measurements have been separated in two groups of AuNPs-BI (10 samplers) and AuNPs-TR (10 samplers), exposing them to a fixed lapses of time ranging a period from one day, up to a maximum exposure of 8 weeks (56 days) and the measured data are reported in Figure 3.

Data reported in Figure 3 shows a stable and reproducible uptake capacity of the used AuNPs over a long range of time showing a linear response. The data indicates also a different behaviour between AuNPs-BI and AuNPs-TR. In particular, we could observe that 100 µg of AuNPs-TR were able to absorb 200 – 300 pg of mercury in one day of exposition. Interestingly, the samplers can be exposed for a period of 5-6 months, without encountering saturation phenomena. Moreover, another important characteristic is given by the linearity observed in the adsorption rate, with a low dispersion of the data, indicating any significant influence given from the turbulence of wind or of other atmospheric parameters on the uptake rate. This behaviour could be explained considering that the AuNPs are not only distributed on the surface of the samplers, but also inside the quartz mesh of the sampler's fibres, giving in this way a reduction in the diffusion rate, as highlighted by SEM observations (see next section, Figure 4).

Surface morphological analysis and determination of chemical composition was performed on AuNPs-TR and AuNPs-BI deposited onto quartz fibres, using scanning electron microscopy supported by dual energy dispersive X-ray spectroscopy (SEM-dEDS) and imaging analysis was provided, as reported in SI (Figure S6) [52,60]. Figure 4 compares the morphological change of functionalized gold nanoparticles dependent on the uptake capacity of elemental gas mercury, before and after thermal treatment at 500°C. The AuNPs-TR deposited on quartz fibres clearly shows a partially evolution of the gold nanoparticles having an average dimension ranging from 15 to 550 nm and active total area of about 0.915 μm^2 respectively (Figure 4a). Different morphological evolution may be observed in Figure 4b for AuNPs-BI, where the average dimension change from 19 nm to 2.2 µm and the active total area 7.265 μm^2. By increasing the magnification of the objects (black dot rectangle), it is possible to observe nanoparticles of

dimension under 15 nm with a spherical shape until 40 nm in size. After the thermal treatment, the AuNPs-TR increases in dimension becoming irregular in shape, probably due to an aggregation effect of the small NPs into large objects, reaching a dimension of about 120 nm, as shown in Figure 4c. Similarly, AuNP-BI nanoparticles have regular spherical shapes with low dimensions, up to 50 nm. An aggregation effect still produces particles of micrometric dimension with row surface surrounded by few survival nanoparticles visible in Figure 4d. The different aggregation effect between AuNPs-BI and AuNPs-TR can be explained in term of the different interparticle distance in the NPs network located on the quartz fibres under thermal treatments [47]. It should be noticed that the growth effect of AuNPs is independent from the dimension of the quartz fibres.

3.2 Adsorbent material characterization

Several critical aspects have been evaluated to investigate the performance of AuNPs-BI and AuNPs-TR, detecting the environmental gaseous mercury, such as the adsorption capacity, the long-term stability and the temporal and spatial resolution. In a preliminary series of measures we observed that, compared to AuNPs-BI, the AuNPs-TR showed a greater capacity to absorb mercury vapor. We have therefore focused our attention on this material.

To characterize the absorption capacity of these samplers a first uptake capacity study was carried out, exposing AuNPs-TR samplers to a saturated mercury vapour concentration (of 14.3 mg m^{-3} i.e. 1.7 ppm) as function of the exposure time, reaching a maximum of 240 minutes of exposition. As reported in Figure 5a, a linear adsorption (up to 120 minutes of exposition) can be observed, reaching an equilibrium phase of saturation of 14 ng Hg° adsorbed for AuNPs-TR.

The data show a high uptake capacity toward the GEM of about 14 ng, in relation to the amount of 100 μg of AuNPs-TR material deposited on the quartz fibres. These results are significant compared to other passive vapour mercury samplers based on gold deposited layers or concentrated AuNPs thick films. A direct comparison of the performance of the materials is difficult given the diversity of the proposed systems. What emerges from the comparison with other works in the literature is a very high adsorption capacity, a prolonged mechanical stability as well as a considerable ease of use [26, 43, 61,62]. Selectivity towards relative humidity (RH) was verified by exposing the AuNPs-TR sampler to a fixed quantity of Hg° (0.664 ng) varying different RH with a fixed exposition time of 30 min, as reported in the Supporting Information section (Fig S7).

Another important feature for these absorbent composite materials is focused on their ability to be renewed for long cycle life. In fact, starting from a relatively low cost preparation of each sampler, estimated in 50 euro cents, this could be further reduced by the reuse of the samplers with a resulting reduction in costs in view of possible applications in monitoring campaigns. In order to test this important aspect, the AuNPs-TR samplers have been stressed with a series of cyclic measurements (adsorption and desorption processes) up to 35 times. Figure 5b indicate the percentage of absorbed GEM by stressing the AuNPs-TR samplers, repeatedly exposed to the same mass of GEM (1.995 ng Hg°) for a fixed time (1 hour). Considering the results of adsorption/desorption of AuNPs-TR it is possible to observe that there is any reduction in the uptake capacity of the adsorbent material towards the GEM, suggesting that no relevant degradation occurred on the sorbent material, allowing their reutilization for more consecutively measurements.

4. Conclusions

In the present work, functionalized AuNPs were deposited on quartz substrates and utilized as total gaseous mercury (TGM) adsorbents, for environmental or indoor use. The absorption properties are strongly related to the specific surface area, morphology, crystallinity and chemical composition of the materials. Consequently, gas detection based on functionalized AuNPs would benefit from a relative grain dimension, high surface-to-volume ratio and increased surface activities [63]. This evidence has shown benefits for AuNPs-TR sampler to be able of absorption gaseous mercury as shown by EDS analysis in SI Figure S6c. When their dimension becomes comparable to an appropriate space charge region, the adsorption and desorption processes are modulated by electron transport properties, resulting in high gas sensitivities to ambient gases [64]. Conversely, their sensing properties often suffer degradation due to growth of the gold NPs reducing the surface activities, as observed in AuNPs-BI.

A high uptake towards the GEM was observed (14 ng Hg° for 100 µg of AuNPs-TR). During the exposures, a good stability and a linear response has been observed. Moreover, according to a series of cyclic exposures and desorption, up to 35 times, any reduction in the uptake capacity of these samplers has been observed. This feature allows the reutilization of the devices and allow a substantial reduction of the production cost (estimated 50 Euro cents for each sample). These studies open new perspectives for the developing of a passive mercury sampler based on functionalized AuNPs, useful for the monitoring of both environmental and indoor vapour mercury. Finally, this adsorbing sample exhibit stability response with time, enhanced recovery properties, reproducibility, and can indeed operate at room temperature. There is still plenty for improvement toward a successful application as a gas monitor device, including the control of morphology and the maximization of the surface and interfacial area. The importance to develop

a sensitive device, able to reveal even very low concentrations of gaseous mercury (i.e. ppt or ppq levels) is very crucial related to the human health monitoring.

Author Contributions

The manuscript was written through the contribution of all authors. All authors have given approval to the final version of the manuscript.

ACKNOWLEDGMENT

The authors gratefully acknowledge the Sapienza University of Rome, (Ateneo Sapienza 2016 and 2017) for financial support. The authors acknowledge Ezio Battaglione (Dep. of Anatomical, Histological, Forensic Medicine and Orthopedics Sciences, Human Anatomy Unit, "Pietro M. Motta" Microscopy Laboratory, Sapienza University of Rome) for him fruitful discussions and experimental help in VP-SEM-dEDS measurements.

References

[1] E.G. Pacyna, J.M. Pacyna, K. Sundseth, J. Munthe, K. Kindbom, S. Wilson, F. Steenhuisen, P. Maxson, Global emission of mercury to the atmosphere from anthropogenic sources in 2005 and projections to 2020, Atmosph. Environm. 44 (2010) 2487–2499.

[2] G. Bjorklund, M. Dadar, J. Mettuer, J. Aaseth, The toxicology of mercury: Current research and emerging trends. Environm. Res. 159 (2017) 545-554.

[3] B. Gworek, W. Dmuchowski, A.H. Baczewska, P. Brągoszewska, O. Bemowska-Kałabun, J. Wrzosek-Jakubowska, Air Contamination by Mercury, Emissions and Transformations—a Review, Water, Air, and Soil Pollution. 228 (2017) 123.

[4] I. Cheng, L. Zhang, H. Mao, Relative contributions of gaseous oxidized mercury and fine and coarse particle-bound mercury to mercury wet deposition at nine monitoring sites in North America, J. Geophys. Res. Atmos. 120 (2015) 8549–8562.

[5] P.A. Ariya, M. Amyot, A. Dastoor, D. Deeds, A. Feinberg, G. Kos, A. Poulain, A. Ryjkov, K. Semeniuk, M. Subir, K. Toyota, Mercury Physicochemical and Biogeochemical Transformation in the Atmosphere and at Atmospheric Interfaces: A Review and Future Directions, Chem. Rev. 115 (2015) 3760-3802.

[6] C.T. Driscoll, R.P. Mason, H.M. Chan, D.J. Jacob, N. Pirrone, Mercury as a global pollutant: sources, pathways, and effects. Environ. Sci. Technol. 47 (2013) 4967–4983.

[7] F. Sprovieri, N. Pirrone, M. Bencardino, F. D'Amore, F. Carbone, S. Cinnirella, et al. Atmospheric mercury concentrations observed at ground-based monitoring sites globally distributed in the framework of the GMOS network. Atmosph. Chem. Phys. 16 (2016) 11915-11935.

[8] J. Wang, L. Zhang, Z. Xie, Total gaseous mercury along a transect from coastal to centralAntarctic: Spatial and diurnal variations, J. Hazard. Mat. 317 (2016) 362–372.

[9] R. Beauvais-Flück, F. Gimbert, O. Méhault, C. Cosio, Trophic fate of inorganic and methyl-mercury in a macrophyte-chironomid food chain. J. Hazard. Mat. 338 (2017) 140–147.

[10] F.M. Rebelo, E.D. Caldas, Arsenic, lead, mercury and cadmium: Toxicity, levels in breast milk and the risks for breastfed infants. Environm. Research 151 (2017) 671-688.

[11] M.M. Rahman, R.J.C. Brown, K.H. Kim, H.O. Yoon, N.T. Phan, Evaluation of the Memory Effect on Gold-Coated Silica Adsorption Tubes Used for the Analysis of Gaseous Mercury by Cold Vapor Atomic Absorption Spectrometry, Scientific World J. 2013 (2013) 1-10.

[12] S.K. Pandey, K.H. Kim, R.J.C. Brown, Measurement techniques for mercury species in ambient air. Trac-Trends in Anal. Chem. 30 (2011) 899–917.

[13] J. Huang, H.D. Choi, M.S. Landis, T.M. Holsen, An application of passive samplers to understand atmospheric mercury concentration and dry deposition spatial distributions. J. Environ. Monit. 14 (2012) 2976-2982.

[14] D.S. McLagan, C.P.J. Mitchell, H. Huang, Y.D. Lai, A.S. Cole, A. Steffen, H. Hung, F. Wania, A High-Precision Passive Air Sampler for Gaseous Mercury. Environ. Sci. Technol. Lett. 3 (2016) 24−29.

[15] W. Zhang, Y. Tong, D. Hu, L. Ou, X. Wang, Characterization of atmospheric mercury concentrations along an urban–rural gradient using a newly developed passive sampler. Atmos. Environm. 1 (2012) 26–32.

[16] M.S. Gustin, H.M. Amos, J. Huang, M.B. Miller, K. Heidecorn, Measuring and modeling mercury in the atmosphere: a critical review. Atmos. Chem. Phys., 15 (2015) 5697–5713.

[17] Y. Sabri, S. Ippolito, J. Tardio, A. Atanacio, D. Sood, S. Bhargava, Mercury Diffusion in Gold and Silver Thin Film Electrodes on Quartz Crystal Microbalance Sensors. Sens. Actuator B 137 (2009) 246−252.

[18] T. Morris, G. Szulczewski, Evaluating the Role of Coinage Metal Films in the Detection of Mercury Vapor by Surface Plasmon Resonance Spectroscopy. Langmuir 18 (2002) 5823−5829.

[19] K.M.M. Kabir, Y.M. Sabri, L. Myers, J. Harrison, E. Boom, V.E. Coyle, S.J. Ippolito, S.K. Bhargava, Investigating the cross-interference effects of alumina refinery process gas species on a SAW based mercury vapor sensor. Hydrometallurgy, 170 (2017) 51–57.

[20] C. Gómez-Giménez, M.T. Izquierdo, M. de las Obras-Loscertales, L.F. de Diego, F. García-Labiano, J. Adánez, Mercury capture by a structured Au/C regenerable sorbent under oxycoal combustion representative and real conditions. Fuel, 207 (2017) 821–829.

[21] K.M.M. Kabir, S.J. Ippolito, A.E. Kandjani, Y.M. Sabri, S.K. Bhargava, Nano-engineered surfaces for mercury vapor sensing: Current state and future possibilities. Trends Anal. Chem. 88 (2017) 77-99.

[22] M. George, W. Glaunsinger, The Electrical and Structural Properties of Gold Films and Mercury-Covered Gold Films. Thin Solid Films 245 (1994) 215−224.

[23] T. Kobiela, B. Nowakowski, R. Duś, The influence of gas phase composition on the process of Au-Hg amalgam formation. Appl. Surf. Sci. 206 (2003) 78-89.

[24] T. Hou, M. Chen, G.W. Greene, R.G. Horn, Mercury Vapor Sorption and Amalgamation with a Thin Gold Film Appl. Mater. Interf. 7 (2015) 23172-23181.

[25] Y.M. Sabri, S.J. Ippolito, J. Tardio, S.K. Bhargava, Study of surface morphology effects on Hg sorption-desorption kinetics on gold thin-films, J. Phys. Chem. C,116 (2012) 2483-2492.

[26] A. Macagnano, V. Perri, E. Zampetti, A.M. Ferretti, F. Sprovieri, N. Pirrone, A. Bearzotti, G. Esposito, F. De Cesare, Elemental mercury vapor chemoresistors employing TIO_2 nanofibers photocatalytically decorated with Au-nanoparticles. Sens. Actuator B 247 (2017) 957–967.

[27] A. Zanotto, R. Matassa, M.L. Saladino, M. Berrettoni, M. Giorgetti, S. Zamponi, E. Caponetti, Cobalt hexacyanoferrate–poly(methyl methacrylate) composite: Synthesis and characterization. Mat. Chem. Phys. 120 (2010) 118-122.

[28] I. Fratoddi, E. Zampetti, I. Venditti, C. Battocchio, M.V. Russo, A. Macagnano, A. Bearzotti, Platinum nanoparticles on electrospun titania nanofibers as hydrogen sensing materials working at room temperature, Nanoscale, 6 (2014) 9177-9184.

[29] S.B. Meital, H. Hossam, Flexible Sensors Based on Nanoparticles. ACS Nano, 7 (2013) 8366–8378.

[30] M. Stratakis, H. Garcia, Catalysis by Supported Gold Nanoparticles: Beyond Aerobic Oxidative Processes. Chem. Rev. 112 (2012) 4469–4506.

[31] I. Venditti, C. Palocci, L. Chronopoulou, I. Fratoddi, L. Fontana, M. Diociaiuti, M.V. Russo, Candida rugosa lipase immobilization on hydrophilic charged gold nanoparticles as promising biocatalysts: activity and stability investigations. Coll. Surf. B, 131 (2015) 96-101.

[32] A. Liu, G. Wang, F. Wang, Y. Zhang, Gold nanostructures with near-infrared plasmonic resonance: Synthesis and surface functionalization. Coord. Chem. Rev. 336 (2017) 28-42.

[33] I. Fratoddi, A. Cartoni, I. Venditti, D. Catone, P. O'Keeffe, A. Paladini, F. Toschi, S. Turchini, F. Sciubba, G. Testa, C. Battocchio, L. Carlini, R. Proietti Zaccaria, E. Magnano, I. Pis, L. Avaldi, Gold nanoparticles functionalized by Rhodamine B Isothiocyanate: a new tool to control Plasmonic Effects, J. Coll. Surf. Sci. 513 (2018) 10-19.

[34] E.C. Dreaden, A.M. Alkilany, X. Huang, C.J. Murphy, M.A. El-Sayed, The Golden Age: Gold Nanoparticles for Biomedicine, Chem. Soc. Rev. 41 (2012) 2740-2779.

[35] L. Dykman, N. Khlebtsov, Gold Nanoparticles in Biomedical Applications: Recent Advances and Perspectives. Chem. Soc. Rev. 41 (2012) 2256-2282.

[36] J.F. Masson, Surface Plasmon Resonance Clinical Biosensors for Medical Diagnostics ACS Sens., 2 (2017) 16–30.

[37] H. Bessar, I. Venditti, L. Benassi, C. Vaschieri, P. Azzoni, G. Pellacani, C. Magnoni, E. Botti, V. Casagrande, M. Federici, A. Costanzo, L. Fontana, G. Testa, F.F. Mostafa, S.A. Ibrahim, M.V. Russo, I. Fratoddi, Functionalized gold nanoparticles for topical delivery of methotrexate for the treatment of psoriasis, Coll. Surf. B: Biointerf. 141 (2016) 141–147.

[38] C. Battocchio, F. Porcaro, S. Mukherjee, E. Magnano, S. Nappini, I. Fratoddi, M. Quintiliani, M.V. Russo, G. Polzonetti, Gold nanoparticles stabilized with aromatic thiols: interaction at the molecule-metal interface and structure of the molecular shell investigated by SR-XPS and NEXAFS, J. Phys. Chem. C, 118 (2014) 8159 – 8168.

[39] S.R.K. Perala, S. Kumar, On the Mechanism of Metal Nanoparticle Synthesis in the Brust-Schiffrin Method. Langmuir, 29 (2013) 9863−9873.

[40] Y.N. Sabri, A.E. Kandjani, S.J. Ippolito, S.K. Bhargava, Nanosphere Monolayer on a Transducer for Enhanced Detection of Gaseous Heavy Metal. ACS Appl. Mater. Interfaces 7 (2015) 1491−1499.

[41] J.Z. James, D. Lucas, C.P. Koshland, Elemental mercury vapor interaction with individual gold nanorods. Analyst, 138 (2013) 2323-2328.

[42] G.V. Ramesh, T.P. Radhakrishnan, A Universal Sensor for Mercury (Hg, HgI, HgII) Based on Silver Nanoparticle-Embedded Polymer Thin Film. ACS Appl. Mater. Interfaces, 3 (2011) 988–994.

[43] J.Z. James, D. Lucas, C.P. Koshland, Gold Nanoparticle Films As Sensitive and Reusable Elemental Mercury Sensors, Environ. Sci. Technol. 46 (2012) 9557–9562.

[44] M. Ozaki, A. Uddin, E. Sasaoka, S. Wu, Temperature programmed decomposition desorption of the mercury species over spent iron-based sorbents for mercury removal from coal derived fuel gas. Fuel 87 (2008) 3610-3615.

[45] F. Vitale, R. Vitaliano, C. Battocchio, I. Fratoddi, E. Piscopiello, L. Tapfer, M.V. Russo, Synthesis and characterization of gold nanoparticles stabilized by Palladium(II) phosphine thiol, J. Organomet. Chem. 693 (2008) 1043-1048.

[46] I. Chakraborty, T. Pradeep, Atomically Precise Clusters of Noble Metals: Emerging Link between Atoms and Nanoparticles. Chem. Rev. 117 (2017) 8208–8271.

[47] M. Quintiliani, M. Bassetti, C. Pasquini, C. Battocchio, M. Rossi, F. Mura, R. Matassa, L. Fontana, M.V. Russo, I. Fratoddi, Network assembly of gold nanoparticles linked through fluorenyl dithiol bridge. J. Mater. Chem. C, 2 (2014) 2517-2527.

[48] L. Fontana, M. Bassetti, C. Battocchio, I. Venditti, I. Fratoddi, Synthesis of gold and silver nanoparticles functionalized with organic dithiols, Coll. Surf. A, 532 (2017) 282-289.

[49] R. Dumarey, R. Heindryckx, R. Dams, J. Hoste, Determination of volatile mercury compounds in air with the coleman mercury analyzer system. Anal. Chim. Acta, 107 (1979) 159-167.

[50] R. Dumarey, E. Temmerman, R. Dams, J. Hoste, The accuracy of the vapour-injection calibration method for the determination of mercury by amalgamation/cold-vapour atomic absorption spectrometry. Anal. Chim. Acta 170 (1985) 337-340.

[51] I. Fratoddi, R. Matassa, L. Fontana, I. Venditti, G. Familiari, C. Battocchio, E. Magnano, S. Nappini, G. Leahu, A. Belardini, R. Li Voti, C. Sibilia, Electronic Properties of a Functionalized Noble Metal Nanoparticles Covalent Network, J. Phys. Chem. C 121 (2017) 18110-18119.

[52] P. Zhang, Z.A. Qiao, X. Jiang, G.M. Veith, S. Dai, Nanoporous Ionic Organic Networks: Stabilizing and Supporting Gold Nanoparticles for Catalysis. Nano Lett. 15 (2015) 823–828.

[53] R. Matassa, G. Familiari, E. Battaglione, C. Sibilia, G. Lehau, A. Belardini, I. Venditti, L. Fontana, I. Fratoddi, Electron Microscopy Reveals Soluble Hybrid Network of Individual Nanocrystal Self-Anchored by Bifunctional Thiol Fluorescent Bridges, Nanoscale 8 (2016) 18161-18169.

[54] L. Fontana, I. Fratoddi, I. Venditti, D. Ksenzov, M.V. Russo, S. Grigorian, Structural studies on drop-cast film based on functionalized gold nanoparticles network: the effect of heating treatment, Appl. Surf. Sci. 369 (2016) 115-119.

[55] F. Vitale, I. Fratoddi, C. Battocchio, E. Piscopiello, L. Tapfer, M.V. Russo, G. Polzonetti, C. Giannini, Mono and bifunctional arenethiols as surfactants for gold nanoparticles: synthesis and characterization, Nanoscale Res.Lett. 6 (2011) 103.

[56] F. Vitale, L. Mirenghi, E. Piscopiello, G. Pellegrini, E. Trave, G. Mattei, I. Fratoddi, M.V. Russo, L. Tapfer, P. Mazzoldi, Gold nanoclusters - organometallic polymer nanocomposites: synthesis and characterization, Mat. Sci. Eng. C, 27 (2007) 1300–1304.

[57] S.K. Ghosh, T. Pal, Interparticle Coupling Effect on the Surface Plasmon Resonance of Gold Nanoparticles: from Theory to Applications. Chem. Rev. 107 (2007) 4797−4862.

[58] S. Zhang, R. Geryak, J. Geldmeier, S. Kim, V.V. Tsukruk, Synthesis, Assembly, and Applications of Hybrid Nanostructures for Biosensing. Chem. Rev. 117 (2017) 12942–13038.

[59] S. Taniguchi, M. Minamoto, M.M. Matsushita, T. Sugawara, Y. Kawadab, D. Bethell, Electron transport in networks of gold nanoparticles connected by oligothiophene molecular wires. J. Mater. Chem. 16 (2006) 3459–3465.

[60] R. Matassa, G. Familiari, M. Relucenti, E. Battaglione, E. Downing, A. Pacella, G. Cametti, P. Ballirano, A Deep Look Into Erionite Fibres: an Electron Microscopy Investigation of their Self-Assembly. Scientific Reports, 5 (2015) 16757.

[61] E.B. Santos, S. Ferlin, A.H. Fostier, I.O. Mazali, Using Gold Nanoparticles as Passive Sampler for Indoor Monitoring of Gaseous Elemental Mercury J. Brazil. Chem. Soc. 28 (2017) 28.

[62] J. Huang, S.N. Lyman, J. Stamenkovic Hartman, M.S. Gustin, A review of passive sampling systems for ambient air mercury measurements. Environ. Sci.: Processes Impacts, 16 (2014) 374-392.

[63] S. Orlanducci, F. Toschi, V. Guglielmotti, I. Cianchetta, C. Magni, E. Tamburri, M.L. Terranova, R. Matassa, M. Rossi, A Viable and Scalable Route for the Homogrowth of Si Nanocones and Si/C Nanostructures. Crystal Growth & Design, 12 (2012) 4473–4478.

[64] R. Matassa, S. Orlanducci, E. Tamburri, V. Guglielmotti, D. Sordi, M.L. Terranova, D. Passeri, M. Rossi, Characterization of carbon structures produced by graphene self-assembly. J. Appl. Crystal. 47 (2014) 222-227.

Figures Captions:

Fig. 1. (a) Chemical structure of AuNPs-BI and (b) AuNPs-TR nanoparticles; and (c) reaction scheme; (d) UV-Vis absorption spectra of AuNPs-BI (black line) and AuNPs-TR (red line) nanoparticles in CH_2Cl_2. The arrow indicates the absorption peak at about 600 nm.

Fig. 2 AFM topography images of deposited AuNPs-TR on a silicon slice support, analyzed before: a, b (1 μm x 1 μm); and after: c, d (10 μm x10 μm) the thermal treatment at 500°C.

Fig. 3 Desorption mercury measurements of the AuNPs-TR (red), AuNPs-BI (black) samplers as a function of exposition time in outdoor environment (up to 56 days). The error bars indicate the standard deviation. Measurements were carried out in triple.

Fig. 4 SEM images of AuNPs deposited onto quartz fibers after thermal treatment: AuNPs-TR (a, c) and AuNPs-BI (b, d).

Fig. 5 a) Uptake capacity of an AuNPs-TR sampler, at different exposition times to saturated mercury vapour (concentration of 14.3 mg m^{-3} - 1.7 ppm). The error bars indicate the instrumental error; b) Cyclic thermal adsorption/desorption of AuNPs-TR samplers show any significant variation in the sensitivity values over time and expositions. The error bars indicate the instrumental error.

Figures:

Fig. 1

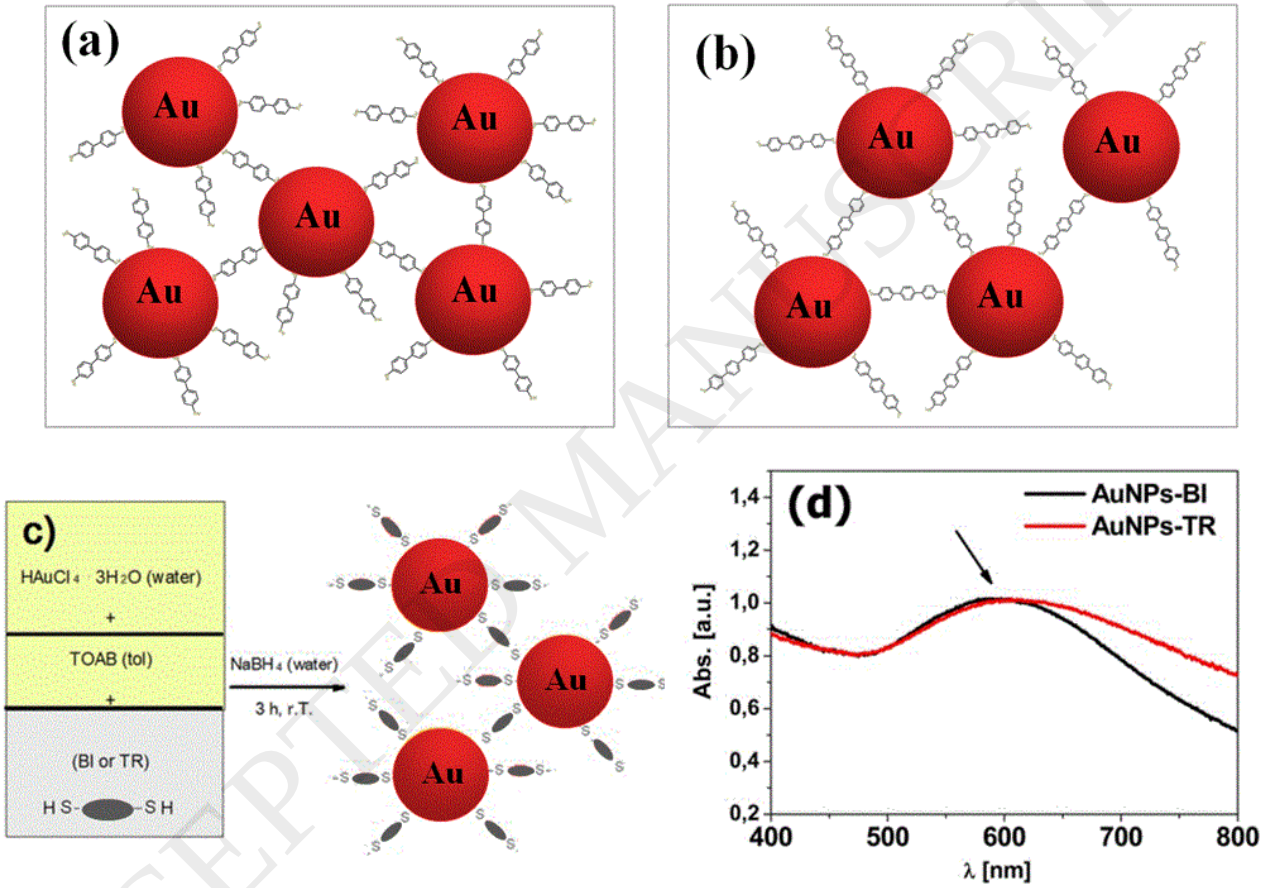

Fig. 2

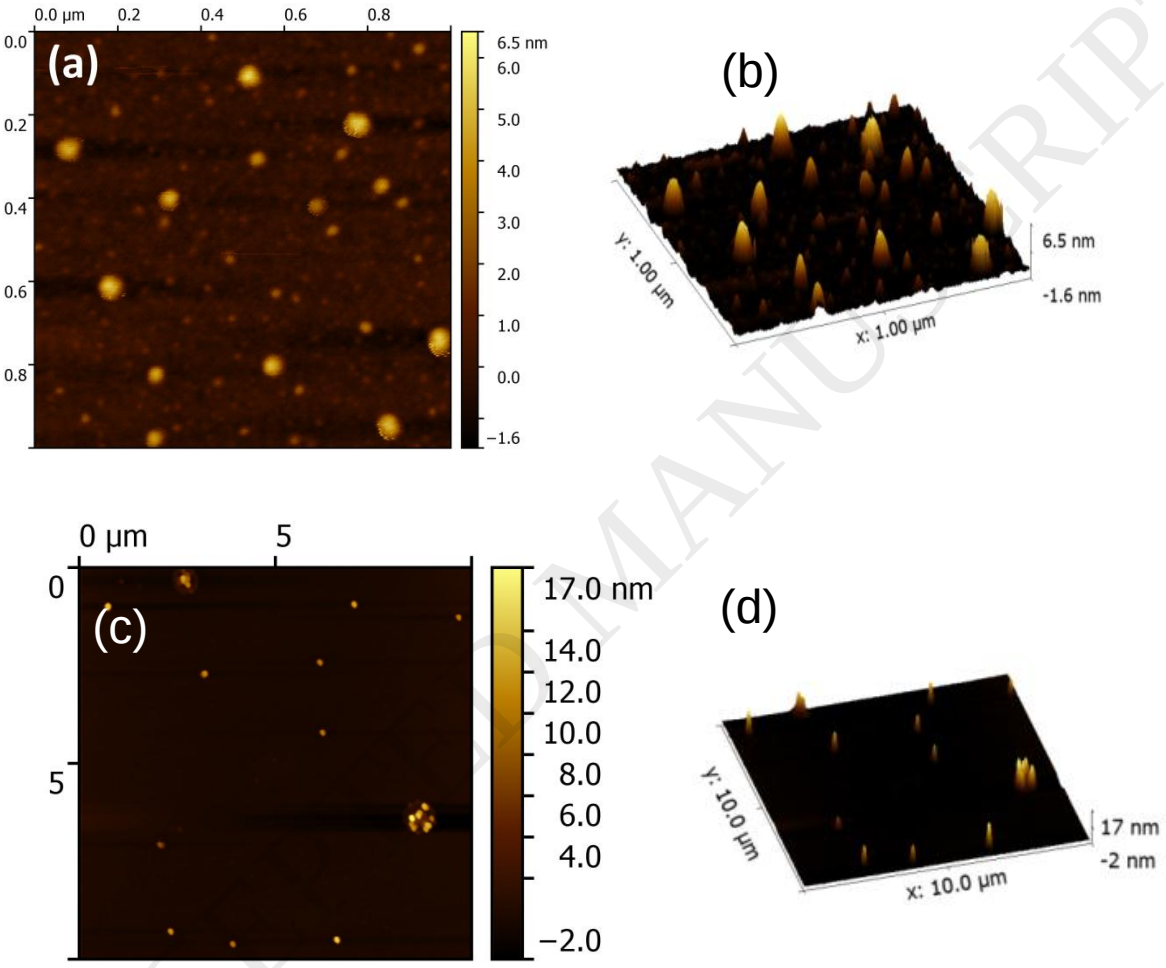

Fig. 3

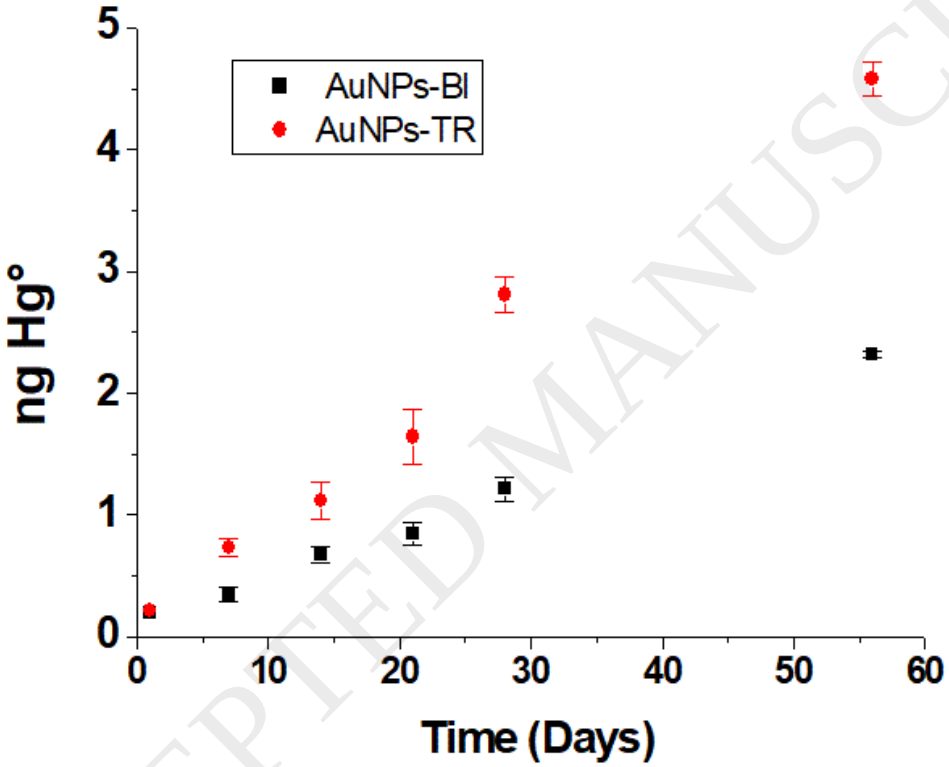

Fig. 4

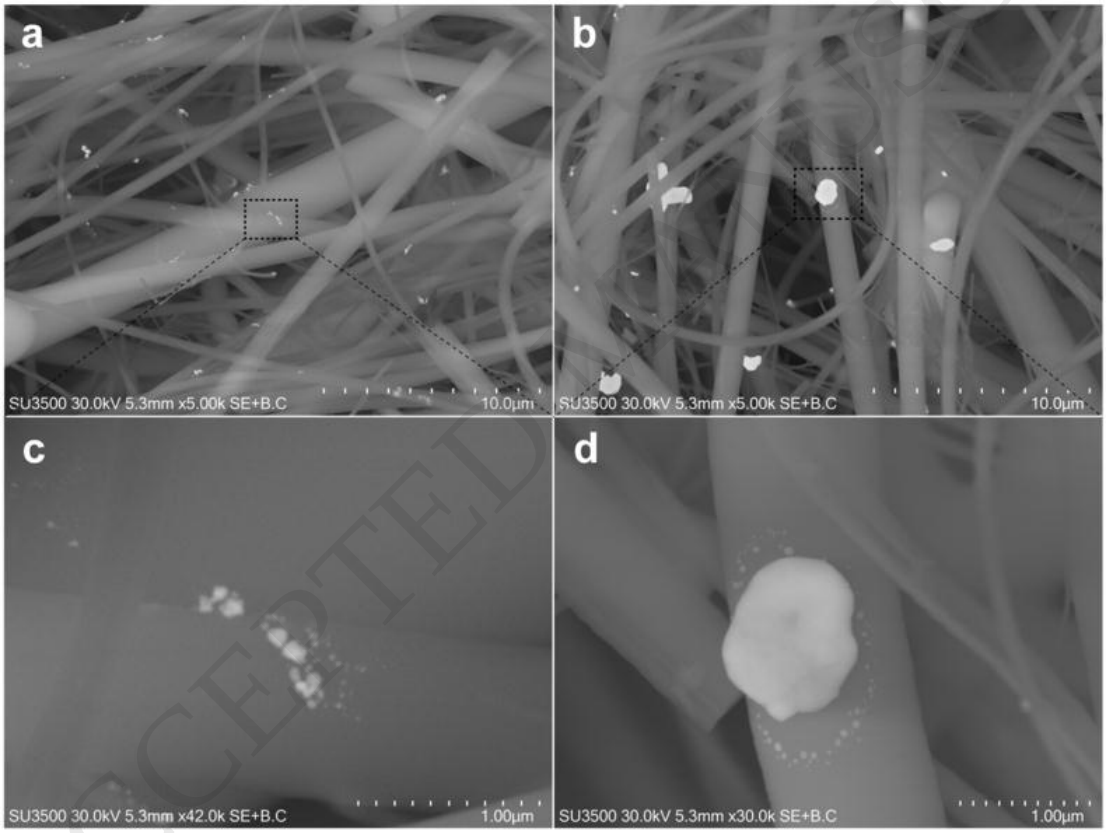

Fig. 5a

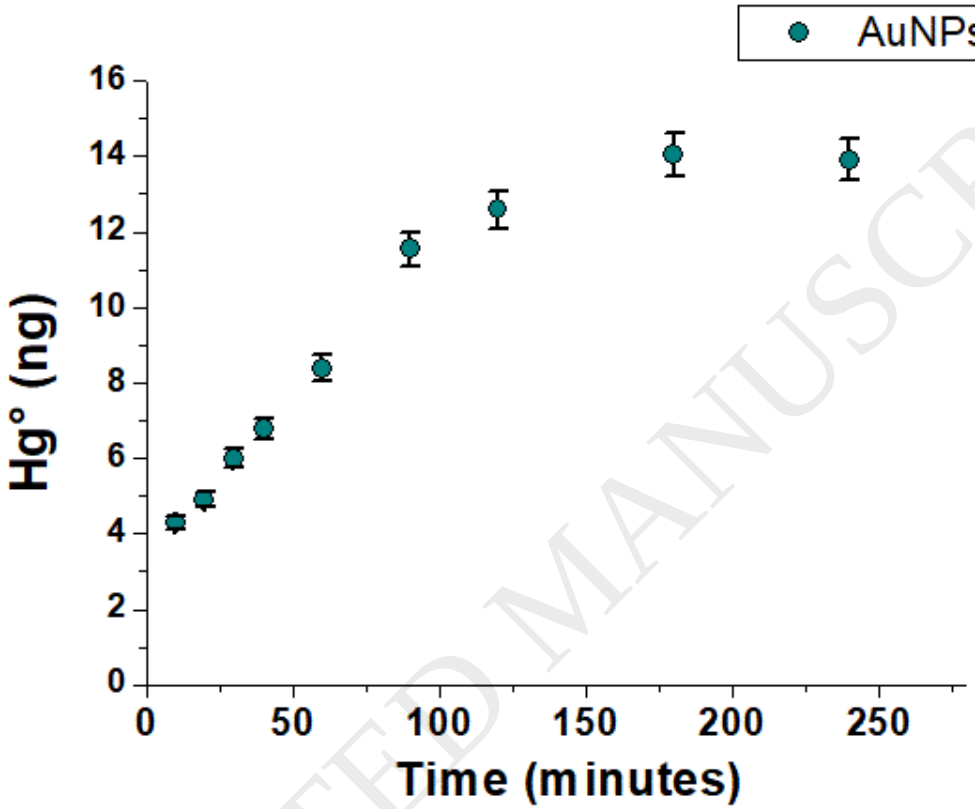

Fig. 5b